Theoretical and Applied Fracture Mechanics 109 (2020) 102685

Contents lists available at ScienceDirect

Theoretical and Applied Fracture Mechanics

journal homepage: www.elsevier.com/locate/tafmec

Investigation of mechanical and fracture properties of wire and arc additively manufactured low carbon steel components

Anna Ermakova[a], Ali Mehmanparast[a,*], Supriyo Ganguly[b], Javad Razavi[c], Filippo Berto[c]

[a] Offshore Renewable Energy Engineering Centre, Cranfield University, England, UK
[b] Welding Engineering and Laser Processing Centre, Cranfield University, Cranfield MK43 0AL, UK
[c] Norwegian University of Science and Technology (NTNU), Trondheim, Norway

ARTICLE INFO

Keywords:
Fracture toughness
Mechanical properties
Structural Integrity
Additive manufacturing
Life assessment
Advanced manufacturing technologies

ABSTRACT

Wire and Arc Additive Manufacturing (WAAM) technology offers efficient fabrication of large scale products and is currently being implemented across various industries. In this study, an experimental investigation has been carried out to characterise the mechanical and fracture properties of WAAM components made of ER70S-6 and ER100S-1 metal wires. Microhardness, tensile and fracture toughness tests have been performed on the specimens extracted from the WAAM built walls which were fabricated using an oscillating pattern. The specimens were extracted from different locations, at the top and bottom of the WAAM walls, in two different orientations with respect to the deposition direction. The results show that the material hardness and yield strength of ER100S-1 built wall are higher than ER70S-6 by 62% and 42%, respectively. Moreover, in the walls made with both materials, the yield and ultimate tensile strength values were found to be slightly higher in specimens extracted in deposition (horizontal) direction when compared to specimens extracted in the built (vertical) direction. The average value of fracture toughness parameter for ER70S-6 has been found to be 88% higher than ER100S-1 material. Furthermore, the results show that the specimen extraction location in ER100S-1 wall significantly influences the fracture toughness values obtained from experiments. The results from this study have been compared with those available in the literature and discussed in terms of the mechanical and fracture properties effects on structural integrity assessment of WAAM components.

1. Introduction

Additive manufacturing (AM) brings a radically new production method that enables functionally superior designs at a lower cost with enhanced productivity, greater sustainability and is set to revolutionise many industries globally. AM can be considered as an alternative fabrication method for complicated engineering components by addressing the current manufacturing challenges and geometrical constraints. The new AM technology enables fabrication of hybrid components with several alloys, which are deposited in the form of powder or wire. Among all existing AM methods, wire and arc additive manufacturing (WAAM) is known as a relatively inexpensive technique that provides the highest deposition rates and is suitable for the fabrication of large size products [1,2]. Using this technique, the deposition process is performed in open air using a robotic arm with a localised shielded area, which indicates an alternative application of this technology for repair processes in remote areas, such as offshore plant [3].

An important challenge in the structural integrity of WAAM components is to evaluate the influence of welding processes embedded into the WAAM technique on mechanical and fracture properties, compared to those of obtained from the wrought material [4]. In addition to the mechanical response, the metallurgical differences such as microstructural variations, locked-in residual stresses, phase formation processes and compositional segregation must be carefully examined and classified before employing such components in critical operational loading conditions.

Mechanical properties of WAAM mild steel specimens were investigated by Haden et al. [5] who showed that the composition of printed steel specimens is comparable with the composition of the wrought steel. Moreover, they showed that the WAAM specimens have the average hardness value of bulk steel. Another study [6] has shown a good agreement between uniaxial tensile trends in WAAM mild steel samples and the wrought low carbon steels, with similar yield strength and ultimate tensile strength (UTS) values. Suryakumar et al. [7] have concluded that tensile properties for printed mild steel specimens can differ by up to 10% for different orientations and showed that tensile

* Corresponding author.
E-mail address: a.mehmanparast@cranfield.ac.uk (A. Mehmanparast).

https://doi.org/10.1016/j.tafmec.2020.102685
Received 1 May 2020; Received in revised form 17 June 2020; Accepted 17 June 2020
Available online 20 June 2020

Nomenclature

a_0	initial crack length in CT specimens
a_i	instantaneous crack length
$a_{i,p}$	crack length after pre-fatigue cracking
$a_{f,c}$	final crack length (compliance data)
$a_{f,op}$	final crack length (fracture surface)
A_p	plastic area
Δa	crack extension
B	total thickness of CT specimens
B_e	effective thickness
B_n	net thickness
C_i	instantaneous unloading compliance
d	gauge diameter
D	gripping diameter
E	Young's modulus
F_{max}	maximum load for pre-fatigue cracking
H	height of CT specimens
J	Elastic-plastic fracture mechanics parameter
J_{IC}	fracture toughness
K	stress intensity factor
L	length of uniaxial cylindrical specimens
P_{max}	maximum load observed in fracture toughness tests
W	width of CT specimens
$\varepsilon_{f,axial}$	axial strain
ε_{ROA}	reduction of area
η	geometry dependent function
ν	Poisson's ratio
σ_{UTS}	ultimate tensile strength
σ_Y	yield stress
AM	Additive Manufacturing
B	Bottom
C(T)	Compact Tension specimen
CMT	Cold Metal Transfer
DIC	Digital Image Correlation
EDM	Electrical Discharge Machining
H	Horizontal
LLD	Load Line Displacement
T	Top
UTS	Ultimate Tensile Strength
V	Vertical
WAAM	Wire + Arc Additive Manufacturing

strength can be improved by increasing the current of welding arc. Titanium specimens extracted from thin WAAM walls were tested by Wang et al. [8], and no correlation was found between the position of the specimen on the wall and the tensile properties. However, it was observed, that the orientation has an impact on the results, reducing yield and UTSs of the vertical specimens. Overall, tensile properties values were similar to the wrought titanium material properties. Similar trends in WAAM titanium specimens were reported by other researchers [9,10].

Fracture toughness tests were conducted on WAAM titanium specimens by Zhang et al. [11], and the results have shown similar or greater values compared with the wrought titanium samples. Moreover, it was observed that the orientation of the specimen significantly affect the fracture toughness properties, which are higher when the crack propagates perpendicular to the deposited layers.

The review of the existing data shows that the majority of the previous studies using the WAAM technique were on titanium, aluminium or stainless steel materials and new studies are needed to comprehensively characterise the mechanical response of WAAM built wall using different steels. Moreover, while the majority of the previous studies were conducted on microstructural and mechanical properties of WAAM built walls, there are limited data available in the literature on fracture behaviour of these components which is a crucial property for life assessment of engineering components under operational loading conditions. Therefore, to fill the gap in the knowledge, the present study investigates the mechanical and fracture properties of WAAM built walls made of two different mild steels. Also included in this study is an examination of the sensitivity of the mechanical response of the WAAM material to the built orientation, and location along the wall height. The specimen preparation process, experimental procedures and test set-up details are described below and the presented results are discussed and compared with the existing data in the literature.

2. Material selection and fabrication process

For the current research two types of mild steel welding wires were selected that are suitable for welding low and medium tensile steels: ER70S-6 and ER100S-1. The ER70S-6 contains deoxidisers that provide better wetting, material yielding and the capacity of faster welding travel speed, which helps support higher productivity and increase consumable life [12]. This material is suitable for welding of steels with moderate amount of imperfections, which makes it a preferred material choice for marine applications [13,14]. However, these ER70S-6 wires tend to generate silicon island deposits on the weld surface that need to be removed prior to surface conditioning such as painting, which may increase the time for post-processing treatments. For the current research, Lincoln Electric ER70S-6 wire was used, with typical composition presented in Table 1. The second material selected for this study is the high toughness ER100S-1 low-alloy steel. This material provides an excellent welding performance and stable arc with the balanced Manganese and Silicon ensuring optimum deoxidisation and weld fluidity [15,16]. The ER100S-1 wire offers outstanding toughness of the weld metal at low temperatures and is suitable for offshore applications. The composition of ER100S-1 material used in this study is shown in Table 1. It is worth noting that ER100S-1 wires are around ten times more expensive than ER70S-6.

In order to build the additively manufactured walls in this study, the Cold Metal Transfer (CMT) based WAAM process was used with the manufacturing parameters presented in Table 2. The same parameters were employed in fabrication of different walls for consistency and in order to minimise structural variability in the final products. The set-up and fabrication process of the WAAM walls is shown in Fig. 1. The base plates selected for this study was the rolled structural steel EN10025 with dimensions of 420 × 200 × 12 mm^3. The deposition of the WAAM walls started at the mid-width of base plates and the layers where deposited on top of each other using an oscillation pattern to obtain a sufficiently thick wall of approximately 24 mm. It has been found in previous studies that the oscillation pattern provides more accurate

Table 1
Chemical composition of materials (wt.-%).

	C	*Mn*	*Cr*	*Si*	*Ni*	*Mo*	*S*	*P*	*Cu*	*V*
ER70S-6	0.09	< 1.60	0.05	0.09	0.05	0.05	0.007	0.007	0.20	0.05
ER100S-1	0.08	1.70	0.20	0.60	1.50	0.50	–	–	–	–

Table 2
CMT-WAAM fabrication parameters.

Shielding gas	Ar + 20% CO_2
Gas flow rate	15 L/min
Robot travelling speed	7.33 mm/sec
Wire diameter	1.2 mm
Wire feed speed	7.5 m/min
Dwell time	120 sec

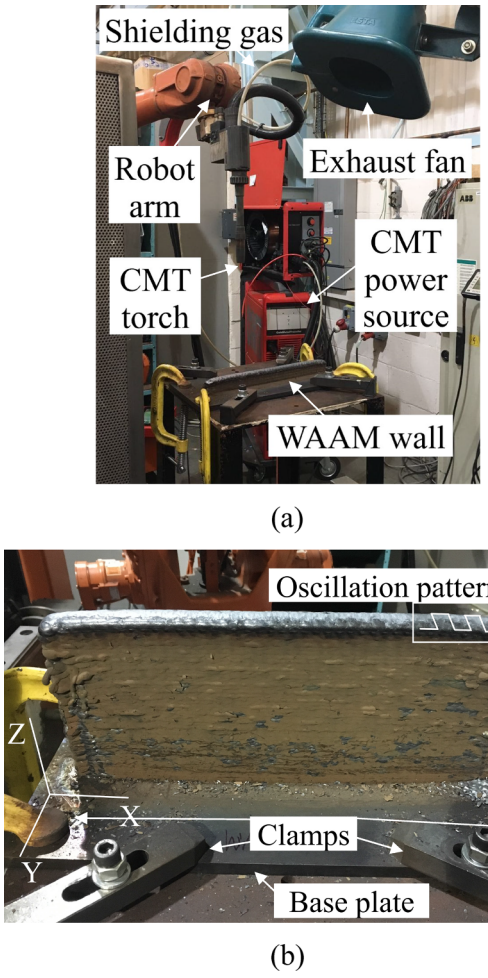

Fig. 1. The fabrication process: (a) CMT WAAM set-up, and (b) completed wall.

control of wall thickness compared to the parallel deposition strategy. Also, since it is a warmer process, it reduces the probability of fusion defects [3]. Moreover, it is less time consuming than depositing multiple straight wiring lines next to each other, turning the arc off and changing the location of the torch, to build a single layer [17,18].

As seen in Fig. 1, the WAAM set-up consists of the CMT power source, a robot arm with the CMT torch feeding the wire along with the pipe that simultaneously supplies shielding gas. Samples fabrication was conducted at the ambient temperature, however, in order to draw off the heat from the sample faster, an exhaust fan was used. The base plate was attached to the working table using eight clamps (two on each side), to minimise distortion of the plate due to the thermal energy input. The clamps were released once the WAAM wall was cooled down to the ambient temperature.

Two walls were manufactured in total, one for each material. The approximate wall dimensions were 355 mm in length (i.e. X-direction in Fig. 1(b)), 24 mm in width (Y-direction in Fig. 1(b)) and 140 mm height (Z-direction in Fig. 1(b))

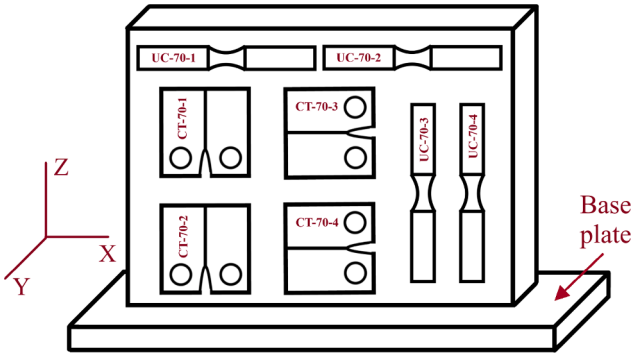

Fig. 2. A schematic demonstration of the specimen extraction plan.

3. Specimen extraction

Upon completion of the WAAM walls fabrication process, compact tension, C(T), test specimens and uniaxial round bars were extracted from the walls using Electrical Discharge Machining (EDM) technique. Moreover, additional cross sectional slices from wall sides, along the height of the walls, were extracted for microhardness measurements. For each of the materials examined in this study, four C(T) and four uniaxial cylindrical specimens were extracted along the two different orientations. As schematically shown in Fig. 2, half of the extracted uniaxial samples had the loading direction perpendicular to the wall height axis (denoted UC-70-1 and UC-70-2), while the other half had a parallel orientation (denoted UC-70-3 and UC-70-4). Similarly, half of the extracted C(T) samples had the crack growth direction parallel to the wall height (denoted CT-70-1 and CT-70-2) while the crack plane in the other half was oriented along the X-direction (denoted CT-70-3 and CT-70-4).

As shown schematically in Fig. 2, for each material and orientation, the C(T) specimens were extracted from the bottom and top of the wall to examine the fracture toughness properties of the WAAM walls with respect to the distance from the base plate. The C(T) specimens were extracted according to ASTM 1820 standard [19] for fracture toughness testing with the width of $W = 50$ mm, the height of $H = 60$ mm, total thickness of $B = 16$ mm, net thickness between the side grooves of $B_n = 12$ mm and initial crack length of $a_0 = 17$ mm before pre-fatigue cracking. The uniaxial cylindrical specimens dimensions were chosen in accordance with ASTM E8 standard [20] with the total length of $L = 112$ mm, gauge diameter of $d = 8$ mm and the gripping diameter of $D = 12$ mm.

4. Mechanical testing and analysis

4.1. Tensile properties

Tensile tests were conducted following ASTM E8M [20] standard on four specimens for each material with two samples per orientation (i.e. vertical and horizontal), to examine the specimen orientation effects on the mechanical properties. All tests were performed under displacement control mode with the rate of 1 mm/min. The strain distribution was measured on the outer surface of the specimens using an extensometer in conjunction with the high-resolution digital image correlation (DIC) technique. It has been reported by various researches that DIC measurements provide an accurate result of local strain variations in tensile tests [21]. During the test, when the specimen is loaded and deforms, the DIC gauge measures displacement by comparing the movement of the reference points in the speckle pattern on the specimen surface. The gauge software tracks the reference points and derives the strain change from local displacement measurements. The tensile tests were carried out at the ambient temperature of around 20 °C. Upon completion of the tests, the average strain values were extracted from the software at

the mid-length of the gauge region to quantify the elastic and plastic tensile properties obtained from each specimen. The average tensile curves between the repeat tests are shown in Fig. 3 for both materials with vertical (V) and horizontal (H) orientations and the results are summarised in Table 3. It can be seen in Fig. 3 and Table 3 that ER70S-6 material has a lower yield stress and greater tensile strain at failure compared to ER100S-1. Also seen in this figure is that for both materials the strain at failure is slightly higher in the horizontal specimen orientation (along the deposited layers) compared to vertical specimens (normal to the deposited layers).

Also included in Table 3 are the elastic Young's modulus, E, yield stress σ_Y (taken as 0.2% proof stress), ultimate tensile strength, σ_{UTS}, and strain at failure which has been calculated based on the axial strain $\varepsilon_{f,axial}$ and reduction of area ε_{ROA}. As seen in this table, the average value of yield stress for ER100S-1 is 42% higher than for ER70S-6 and whereas the UTS for ER100S-1 is about 56% higher. The yield stress for the vertical specimen is lower than for horizontal by 6.8% for ER70S-6 material and is very similar in both orientations for ER100S-1. It can be seen in Table 3 that for both materials, the values of yield stress from both orientations are considerably lower than the values provided in the steel wire datasheets. The tensile curves show similar values of UTS for different specimen orientations though slightly lower in vertical compared to horizontal samples. The strain at failure values, calculated using the radial and axial strain measurements, show lower values for ER100S-1 material than for ER70S-6, which confirms that ER70S-6 is more ductile that ER100S-1. Also seen in the tensile test results is that both materials similar values of $\varepsilon_{f,axial}$ and ε_{ROA} are found in the horizontal and vertical specimens. Finally, the results in Table 3 show that the strain values at failure obtained from the reduction of area measurements are higher than axial measurements. This is due to the fact that the local deformation of the sample is accounted for in the calculation of ε_{ROA}, whereas averaged axial strains are accounted for in the calculation of $\varepsilon_{f,axial}$.

4.2. Microhardness tests

Microhardness measurements were carried out according to BS EN ISO 6507-1:1997 [22]. The hardness tests were set up with a traverse along a straight line in the mid thickness of the walls, with incremental measurements of 2 mm. Fig. 4(a) presents the macro structure of the offcut sample that was etched using 5% Nital solution, revealing the deposited layers. The microhardness tests were conducted with 500 g and 2000 g loads and the results are shown in Fig. 4(b). Also included in this figure are the average hardness values obtained from each load level. Knowing that the height of individually deposited layers is on average about 3 mm (see Fig. 4(a)), it can be observed that the hardness values vary from one layer to another. This fluctuation in hardness values is more pronounced in ER100S-1 sample and can be attributed to local variations in material properties due to the deposition process which can result in segregation of solute atoms within the deposit and lead to different phase formations (Note: ER100S-1 has much higher hardenability than ER70S-6). Also seen in the hardness results is that there is a good agreement between the observed trends obtained under 500 g and 2000 g applied loads with a slight shift to the left as the load increases. The average values of hardness for each material are calculated and summarised in Table 4. From the table, it can be seen that ER100S-1 material is 62% harder than ER70S-6.

The overall hardness patterns show that there is a slight hardening trend in the ER70S-6 alloy near the bottom of the wall and the hardness value increases at the top of the wall, whereas for ER100S-1 it is almost a constant trend throughout the wall height within the inherent experimental scatter. The variation in the hardness values between the middle and bottom of the ER70S-6 wall can be attributed to the effects of the thermal cycles on the mechanical behaviour of the WAAM built wall. As seen in Table 3, the ER70S-6 WAAM built wall demonstrates lower values of yield stress in both orientations compared to ER100S-1. Therefore, the thermal cycling has exhibited a more pronounced effect in the material with a lower yield stress. On the other hand, due to the higher yield stress in ER100S-1, there is no noticeable trend observed between the top and bottom layers on the wall made of this material. It must be noted that ER100S-1 has much higher hardenability than ER70S-6 which results in formation of martensite/bainite type structures (although not as high as medium/high carbon martensite) that would partially temper from the heat of subsequent passes – however, there is no significant hardness variation in the examined ER100S-1 WAAM wall probably because of the complex process of martensite formation and tempering occurring throughout the deposit.

5. Fracture toughness testing and analysis

5.1. Specimen preparation

Fracture toughness tests were conducted on the extracted C(T) specimens using the single specimen compliance measurement-based approach following ASTM 1820 [19] standard. For each material, the tests were performed on four stepped notched specimens; two with vertical and two with horizontal orientation. For each material and orientation, one test was conducted on a sample extracted from the top of the WAAM wall (denoted by T) while the second test was performed on a sample extracted from the bottom of the wall (denoted by B). The fracture toughness specimens made of ER70S-6 and ER100S-1 materials are denoted as CT-70-1 – CT-70-4 and CT-100-1 – CT-100-4. Subsequent to specimen manufacture and prior to testing, all specimens were pre-cracked under fatigue loading using the load-decreasing approach to approximately 32 mm (a/W = 0.64) which is within the allowable range for fracture toughness testing specified in ASTM 1820 [19]. The starting fatigue pre-cracking load was maintained below the maximum allowable load calculated according to Eq. (1) [19]. The purpose of fatigue pre- cracking was to introduce an infinitely sharp crack tip ahead of the machined notch without developing a significant plastic zone size ahead of the crack tip.

$$F_{\max} = \frac{0.4B(W-a_0)^2\sigma_Y}{2W+a_0} \quad (1)$$

It is worth noting that ASTM 1820 [19] recommends to pre-fatigue crack the plane sided samples first and then introduce the required percentage of side grooves into the test specimens. However, since the specimens were created using the WAAM technique, the trial tests on

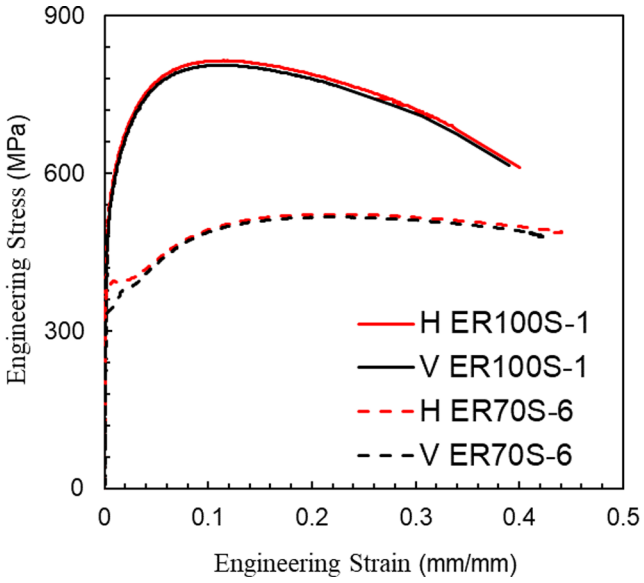

Fig. 3. Engineering stress-strain curves for the two studied materials.

Table 3
A summary of tensile test results.

	ER70S-6			ER100S-1		
	Wire Datasheet	Horizontal	Vertical	Wire Datasheet	Horizontal	Vertical
σ_Y (MPa)	450	390	365	717	538	536
σ_{UTS} (MPa)	540	522	518	780	818	815
E (GPa)	–	209	221	–	181	155
ε_{ROA} (mm/mm)	–	0.77	0.71	–	0.62	0.65
$\varepsilon_{f,axial}$ (mm/mm)	–	0.44	0.43	–	0.40	0.39

dummy samples revealed that maintaining a straight crack path during pre-fatigue cracking was highly challenging and deviations from the straight lines were observed in some dummy samples. Therefore, it was decided to side groove the specimens first and then pre-fatigue crack the samples to maintain a straight started crack and ensure that valid fracture toughness results are obtained from the experiments. The 16 mm thick C(T) specimens were side grooved from both sides by 0.25B (i.e. 25% of the total thickness) which resulted in a net thickness of $B_n = 12$ mm.

5.2. Crack length estimation and J parameter calculation

The estimation of instantaneous crack length in both preliminary fatigue pre-cracking and fracture toughness testing was carried out using the compliance technique and by attaching a clip gauge onto the crack mouth of the specimen. In this approach, the load-line-displacement (LLD) is continuously monitored during the test and the instantaneous crack length is calculated using the elastic compliance measurements following Eqs. (2)–(4) where a_i is the instantaneous crack length, C_i is the instantaneous unloading compliance, E is the elastic Young's modulus and B_e is the effective thickness which is calculated using the specimen full thickness B and net thickness value B_n.

$$\frac{a_i}{W} = 1.000196 - 4.06319u + 11.242u^2 - 106.043u^3 + 464.335u^4 - 650.677u^5 \quad (2)$$

where

$$u = \frac{1}{[B_e E C_i]^{\frac{1}{2}} + 1} \quad (3)$$

$$B_e = B - (B - B_n)^2/B \quad (4)$$

Table 4
Hardness values.

Applied load (g)	ER70S-6	ER100S-1
500	158 ± 14 HV	257 ± 22 HV
2000	151 ± 12 HV	245 ± 18 HV

Fracture toughness tests were performed on a servo-hydraulic machine with the load carrying capacity of 100 kN. The tests were conducted under LLD control mode, by applying the sequences of loading and unloading with 60 s of hold time at each peak load followed by 20% unloading with respect to the peak load value. The loading/unloading rate in all fracture toughness tests was 1 mm/min and the sequences of unloading were conducted at LLD intervals of 0.125 mm. All tests were carried out at room temperature. In order to build up a resistance curve (i.e. R-curve) for fracture toughness analysis, the elastic-plastic fracture mechanics parameter J was calculated using Eq. (5) that is recommended by ASTM 1820 [19]. As seen in this equation, the total value of J is calculated by partitioning it into an elastic and a plastic term which are calculated using Eq. (6) and Eq. (7), respectively. In Eqs. (6) and (7), K is the stress intensity factor the solutions of which are available in the textbooks for different geometries [23], ν is the Poisson's ratio, a_0 is the initial crack length, A_p is the plastic area under the load *vs.* LLD curve and η is a geometry dependent function, the solution of which for C(T) specimen geometry is specified in Eq. (8).

$$J = J_{el} + J_{pl} \quad (5)$$

where

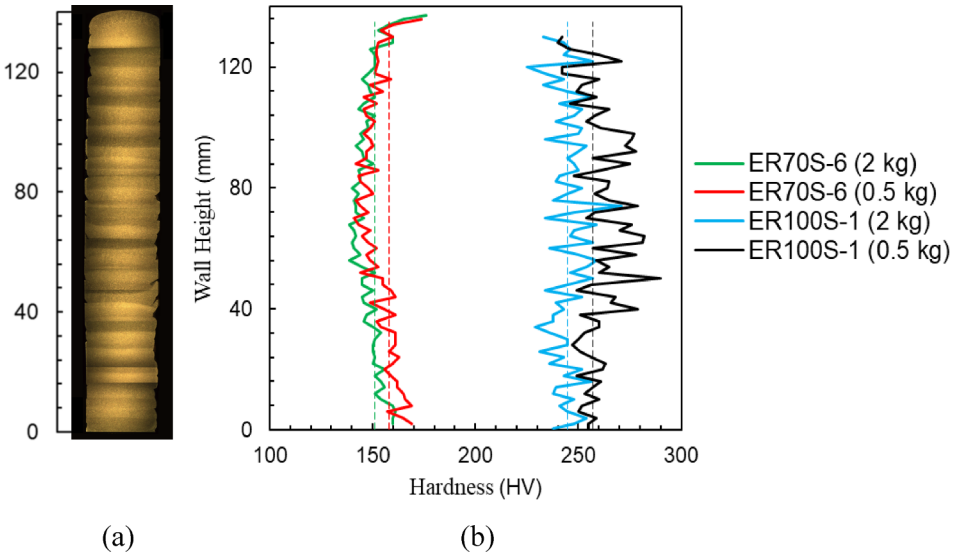

Fig. 4. (a) Macro structure of WAAM wall (b) Hardness test results for WAAM build walls.

$$J_{el} = \frac{K^2(1-\nu^2)}{E} \tag{6}$$

$$J_{pl} = \frac{A_p}{B_n(W-a_0)}\eta \tag{7}$$

$$\eta = 2 + 0.522(W-a_0)/W \tag{8}$$

In order to evaluate the fracture toughness value, the *R*-curve is generated for each test by plotting *J* values against the crack extension, Δa. A blunting line is then constructed (i.e. also referred to as the construction line), the slope of which is estimated using Eq. (9). Subsequently, two exclusion lines are constructed parallel to the blunting line, offsetting the abscissa at 0.15 mm and 1.5 mm. The data points along the *R*-curve that fall in between these two exclusion lines are considered valid and a line of best fit is made to them. The intersection between the line of best fit and a 0.2 mm offset line parallel to the blunting line defines the fracture toughness value which is referred to as J_{IC}.

$$J = 2\sigma_Y \Delta a \tag{9}$$

5.3. Fracture toughness results

The load *vs.* LLD data obtained from all the fracture toughness tests conducted on ER70S-6 and ER100S-1 specimens are shown in Figs. 5 and 6, respectively. The comparison of these two figures shows that the deviation from linearity occurs at a much higher load level in ER100S-1 than ER70S-6, due to the higher yield stress. Also seen in these figures is that upon reaching the maximum load, P_{max}, for each increment of load line displacement, the reduction in the corresponding load level occurs at a much higher rate in ER100S-1 than ER70S-6. Finally seen in these figures is that while similar load *vs.* LLD trends are observed in the tests on ER70S-6 material, more noticeable differences can be observed in the test data on ER100S-1 material. It can be seen in Fig. 6 that the sample extracted with the vertical orientation from the bottom of the wall shows the lowest load *vs.* LLD trend while the sample with horizontal orientation extracted from the top of the wall is exhibiting the highest trend. Finally, it can be seen in these figures that the specimens extracted from the bottom of the wall in both orientations generally show a lower trend compared to those of extracted from the top of the walls indicating the importance the specimens location and orientation of the fracture toughness values in WAAM build components.

The fracture toughness *R*-curves generated for all specimens are presented in Fig. 7, and the J_{IC} values are summarised in Table 5. Also, an example of the detailed fracture toughness analysis by constructing the blunting line, applying the exclusion lines and applying a line of best fit to the valid data points is given in Fig. 8. It can be seen in Fig. 7 that the *R*-curves for the specimens extracted from ER70S-6 show a much higher trend than ER100S-1 meaning that much more energy is required to propagate the crack in specimens made of WAAM ER70S-6 material. This observation is consistent with the fracture toughness values summarised in Table 5 which are on average around nine times higher in ER70S-6 material compared to ER100S-1 (i.e. the average J_{IC} values for ER70S-6 and ER100S-1 are 420.11 kJ/m^2 and 49.19 kJ/m^2, respectively). Also seen in Fig. 7 is that for ER100S-1 material, the specimens extracted from the bottom of the WAAM wall show noticeably lower trends than those extracted from the top of the wall. Detailed comparison of the fracture toughness values in Table 5 shows that for ER70S-6, all fracture toughness values are similar to each other except the vertical sample extracted from the bottom of the wall. Finally seen in Table 5 is that for ER100S-1, while the samples extracted from the bottom of the wall exhibit a noticeably lower fracture toughness value (48% lower), the specimens with vertical orientations have lower fracture toughness values compared to the horizontal samples. This means that similar to ER70S-6, the lowest value of fracture toughness for ER100S-1 is observed for vertical orientation at the bottom of the WAAM wall. These observations on the *R*-curves are consistent with the load *vs.* LLD trends seen in Fig. 5 for ER70S-6 specimens and Fig. 6 for ER100S-1.

The lower resistance curves and fracture toughness values observed at the bottom of the WAAM walls can be attributed to the higher number of thermal cycles at the bottom layers of the WAAM walls which may alter the fracture properties of the built geometry at the bottom sections compared to the top. In order to better understand the thermal cycles effects on the microstructural deformation and fracture behaviour of the WAAM walls, further investigations will be conducted in future work to examine the effect of repeated thermal cycles on the microstructural variations and macro-scale deformation and fracture behaviour of the material.

5.4. Fractography

In order to evaluate the percentage of error in crack extension values obtained using the compliance technique, post-mortem analysis was conducted on all tested fracture toughness specimens. Subsequent to completion of the fracture toughness tests, all eight specimens were soaked in liquid nitrogen to facilitate the fast fracture process. Once the temperature on the samples was sufficiently reduced, the specimens were separated by applying a monotonic loading condition using the hydraulic machine. High resolution macroscopic pictures of the two fracture surfaces of each specimen are shown in Fig. 9. As shown in Fig. 9(a), three surface areas namely (1) the pre-fatigue cracking region, (2) fracture toughness region, and (3) fast fracture region have been identified and the crack extensions in these areas have been measured for each of the test specimens.

It can be seen in Fig. 9 that the cup and cone feature is evident in ER70S-6 specimens, whereas ER100S-1 specimens exhibit a relatively flat fracture surface. Moreover, it can be noted that vertical specimens (with the crack path going across the WAAM layers) have a wavy pre-fatigue cracking surface, which represents different layers. Also symmetric crack propagation regions can be seen in the fractography analysis which confirms that appropriate alignment was maintained during the fracture toughness tests. The key specimen dimensions together with the machined crack length a_o, initial crack length after pre-fatigue cracking (estimated from the compliance data) $a_{i,p}$, the final crack length estimated from the compliance data $a_{f,c}$, and final crack length measured on the fracture surface, $a_{f,op}$ are summarised in Table 6. Also included in this table is the percentage of error between the measured

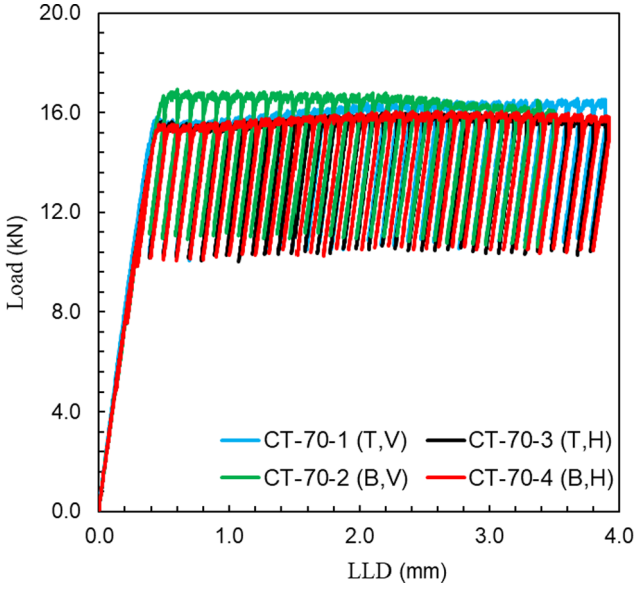

Fig. 5. Load *vs.* LLD for ER70S-6 specimens.

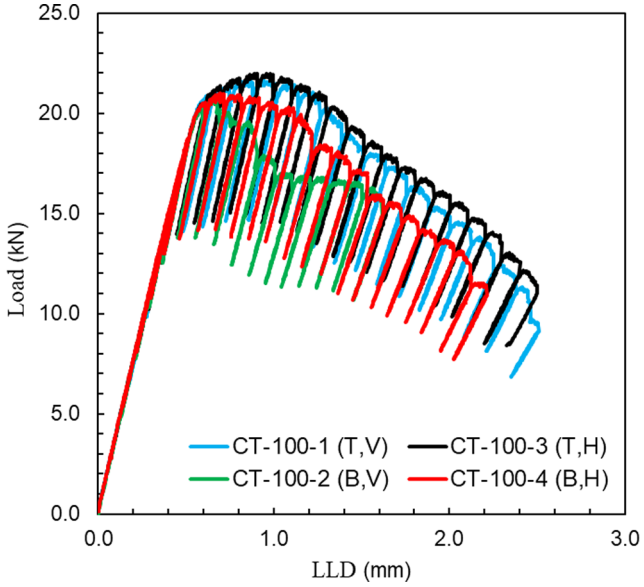

Fig. 6. Load *vs.* LLD for ER100S-1 specimens.

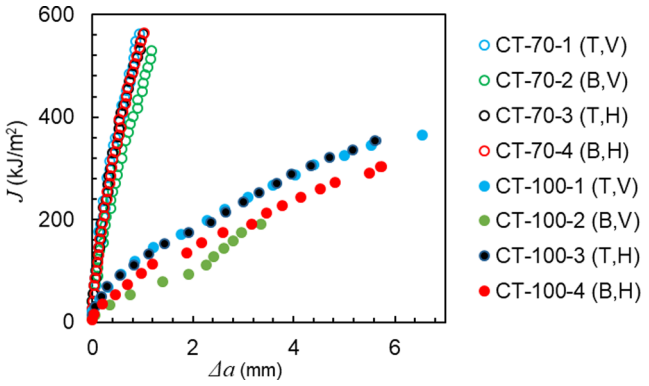

Fig. 7. Resistance curves for ER70S-6 and ER100S-1 specimens.

and estimated final crack lengths. In can be seen in the table that the error is below 9% for all specimens, which confirms that accurate enough estimations were made using the compliance data during the fracture toughness testing process.

6. Discussion

The ER70S-6 specimens examined in the present study show hardness values ranging from 137 to 180 HV, with the yield stress ranging from 365 to 390 MPa and the UTS values varied from 518 to 522 MPa. The obtained data from these experiments are in good agreement with the data provided in the literature [5,24], though some researchers have reported higher or lower values [17,25], which may be particularly because of the different WAAM parameters selected for the fabrication of the walls. Moreover, the average fracture toughness result obtained in this study on ER70S-6 is 420.11 kJ/m^2 which is slightly lower than the result found in the literature for this material [17]. The specimens made with ER100S-1 provide hardness values ranging from

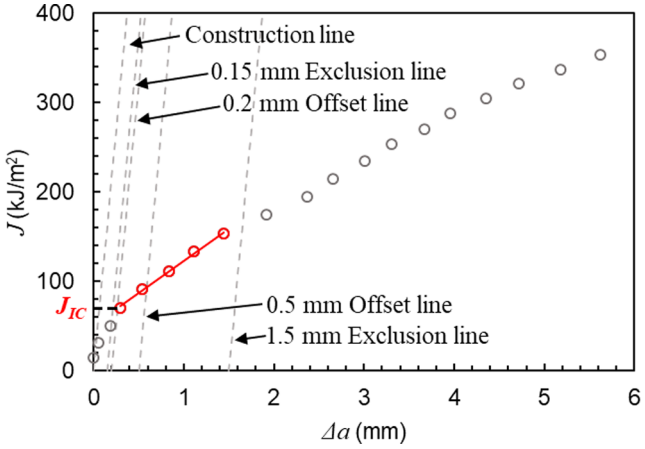

Fig. 8. Analysis of the fracture toughness data for CT-100-3 specimen.

222 to 290 HV, with the yield stress ranging from 536 to 538 MPa, accompanied by UTS values varying from 815 to 818 MPa. The average fracture toughness obtained for these specimens was 91.19 kJ/m^2. No data on the mechanical or fracture toughness properties of WAAM ER100S-1 material was found in the literature for comparison.

The study of different orientations in the current research has shown that regardless of the material employed in the WAAM process, both values of yield stress and σ_{UTS} are higher for horizontal specimens than for vertical. It must be noted that only two specimens per orientation were tested in this study, thus more tests need to be conducted in future work to examine the level of inherent experimental scatter in the mechanical properties obtained for each specimen orientation. This was also reported by several other authors [5,17,6]. Another interesting observation is that the strain at failure is similar in horizontal and vertical specimens for both materials. As for the fracture toughness results, the orientation and specimen extraction location have been found more influential on ER100S-1 than ER70S-6. The comparison of the two materials shows that ER100S-1 has more brittle behaviour compared with ER70S-6 that is more ductile. This can be concluded from the mechanical properties, along with the examination of the fracture surfaces. The fluctuation of hardness values through the WAAM layers is more pronounced for ER100S-1 offcuts. Another observation that can be made from the present study is that the yield stress and hardness values are proportional to each other, as suggested in the literature [26].

The results presented above on WAAM samples have been compared with characteristics of widely used wrought structural metals in Table 7, where the average values of mechanical and fracture properties are presented. These wrought metallic materials include, S355 which is widely used in fabrication of offshore structures [26,27], SS316 which is widely used in high temperature components [28,29] and Aluminium which is often employed in lightweight structures [30]. It can be seen in this table that with the highest values of hardness, yield stress and ultimate tensile stress, ER100S-1 shows slightly higher fracture toughness results than aluminium, however this value is much less than that of observed in S355 steel. On the other hand ER70S-6 values of yield stress and ultimate tensile stress are comparable with S355 and SS316 steels, however the fracture toughness value is lower by around 50% and 25%, respectively. The comparison of the mechanical and fracture properties

Table 5
Fracture toughness values for ER70S-6 and ER100S-1 specimens.

	CT-70-1 (T, V)	CT-70-2 (B, V)	CT-70-3 (T, H)	CT-70-4 (B, H)	CT-100-1 (T, V)	CT-100-2 (B, V)	CT-100-3 (T, H)	CT-100-4 (B, H)
J_{IC} (kJ/m^2)	474.08	312.05	449.16	445.15	62.02	28.68	68.05	38.01

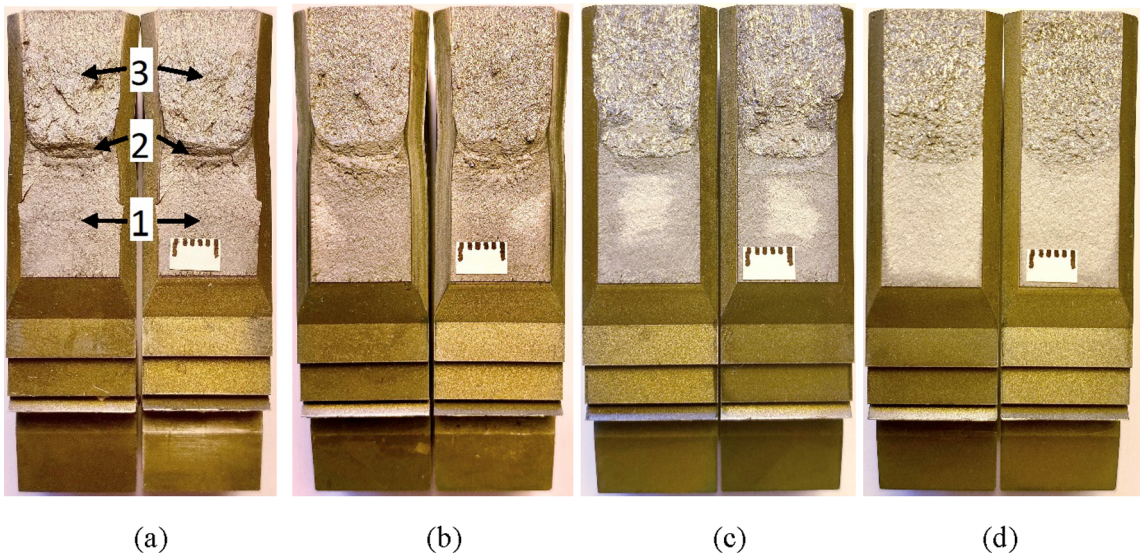

Fig. 9. Fracture surface for ER70S-6 specimen: (a) vertical CT-70-1, (b) horizontal CT-70-3; ER100S-1: (c) vertical CT-100-1, (d) horizontal CT-100-3.

of WAAM built components and wrought metals in Table 7 provides a useful insight into material selection for specific engineering applications where relatively high yield or fracture properties are required to ensure that the designed component tolerates the operational loading conditions during the service life.

In order to fully characterise ER70S-6 and ER100S-1 WAAM walls for various industrial applications, fatigue crack initiation and propagation tests will be performed on specimens with different orientations and extraction locations in the future work. Moreover, residual stresses will be measured in the WAAM walls and extracted specimens to account for their effects on the fatigue behaviour of the WAAM walls made of both materials. It is known that different surface treatment techniques, such as rolling and shot peening, can significantly improve the fatigue performance of WAAM built geometries [31], therefore these fatigue life enhancement techniques will also be investigated in the future work for the WAAM components characterised in the present study. Comprehensive metallurgical analysis of the WAAM walls will be carried out in future work to investigate the correlation between hardness variations and metallurgical features in the WAAM walls.

Table 7
Comparison of mechanical and fracture properties of WAAM specimens with widely used wrought metals.

Material	E (GPa)	σ_Y (MPa)	σ_{UTS} (MPa)	*Hardness* (HV)	J_{IC} (kJ/m^2)
S355 [26,27]	198	446	546	198	830
SS316 [28,29]	205	313	603	155	560
Aluminium [30]	72	503	564	175	29
ER70S-6	215	378	520	155	420
ER100S-1	168	537	817	251	49

7. Conclusions

Material characterisation tests have been conducted on specimens fabricated using WAAM technique with ER70S-6 and ER100S-1 materials. The results have revealed that the average hardness value on ER70S-6 steel specimens is 155 HV which is 61% lower than the value obtained for ER100S-1. Moreover, at the top and bottom of the WAAM walls, higher hardness values are observed for ER70S-6 material, whereas the hardness values in ER100S-1 material were almost uniform. The results have also shown that lower yield stress and UTS values were observed in specimens made of ER70S-6, which have exhibited the higher average fracture toughness compared to ER100S-1 samples, confirming that the values of yield stress and hardness are proportional to each other and inversely proportional to fracture toughness. A trend was discovered for both materials that yield stress and UTS values are similar for different specimen orientations though slightly lower in vertical orientation compared to horizontal samples extracted across the WAAM layers. The specimen orientation does not significantly affect the fracture toughness results in both materials, however, for ER100S-1 the specimen extraction location has been found to have a significant effect on fracture toughness with specimens extracted from the top of the wall showing 48% higher value compared to those extracted from the bottom of the WAAM wall.

Table 6
Specimen dimensions and the initial and final crack lengths.

Specimen ID	W (mm)	B (mm)	B_n (mm)	a_0 (mm)	$a_{i,p}$ (mm)	$a_{f,c}$ (mm)	$a_{f,op}$ (mm)	*% error in* a_f
CT-70-1	50.1	16.0	12.2	17.0	31.6	32.2	35.0	8.0
CT-70-2	50.0	16.1	12.2	17.1	30.3	32.9	33.7	2.3
CT-70-3	50.0	16.0	12.2	17.0	31.3	32.8	33.6	2.5
CT-70-4	50.0	16.0	12.2	17.2	31.5	32.8	33.8	3.0
CT-100-1	50.1	16.2	12.1	17.1	32.4	38.3	38.6	0.6
CT-100-2	50.0	16.1	12.1	17.0	31.5	35.2	35.8	1.7
CT-100-3	50.2	16.0	12.1	17.1	31.7	37.4	41.1	9.0
CT-100-4	50.0	16.2	12.1	17.0	31.5	37.6	37.1	1.2

CRediT authorship contribution statement

Anna Ermakova: Methodology, Formal analysis. **Ali Mehmanparast:** Conceptualization, Supervision, Writing - review & editing. **Supriyo Ganguly:** Formal analysis, Writing - review & editing. **Javad Razavi:** Formal analysis, Writing - review & editing. **Filippo Berto:** Writing - review & editing.

Declaration of Competing Interest

The authors declare that they have no known competing financial interests or personal relationships that could have appeared to influence the work reported in this paper.

Acknowledgements

This work was supported by grant EP/L016303/1 for Cranfield, Oxford and Strathclyde Universities' Centre for Doctoral Training in Renewable Energy Marine Structures – REMS CDT (http://www.rems-cdt.ac.uk/) from the UK Engineering and Physical Sciences Research Council (EPSRC).

References

[1] S.W. Williams, F. Martina, A.C. Addison, J. Ding, G. Pardal, P. Colegrove, Wire + arc additive manufacturing, Mater. Sci. Technol. 32 (2016) 641–647.
[2] J.V. Gordon, C.V. Haden, H.F. Nied, R.P. Vinci, D.G. Harlow, Fatigue crack growth anisotropy, texture and residual stress in austenitic steel made by wire and arc additive manufacturing, Mater. Sci. Eng., A 724 (2018) 431–438.
[3] Y.K. Bandari, T.O. Charrett, F. Michel, J. Ding, S.W. Williams, R.P. Tatum, Compensation strategies for robotic motion errors for additive manufacturing, Solid Free. Fabr. 1–14 (2016).
[4] M. Zhang, C.N. Sun, X. Zhang, P.C. Goh, J. Wei, D. Hardacre, H. Li, Fatigue and fracture behaviour of laser powder bed fusion stainless steel 316L: influence of processing parameters, Mater. Sci. Eng., A 703 (2017) 251–261.
[5] C.V. Haden, G. Zeng, F.M. Carter III, C. Ruhl, B.A. Krick, D.G. Harlow, Wire and arc additive manufactured steel: tensile and wear properties, Addit. Manuf. 16 (2017) 115–123.
[6] X. Lu, Y.F. Zhou, X.L. Xing, L.Y. Shao, Q.X. Yang, S.Y. Gao, Open-source wire and arc additive manufacturing system: formability, microstructures, and mechanical properties, Int. J. Adv. Manuf. Technol. 93 (2017) 2145–2154.
[7] S. Suryakumar, K.P. Karunakaran, U. Chandrasekhar, M.A. Somashekara, A study of the mechanical properties of objects built through weld-deposition, Proc. Inst. Mech. Eng. Part B J. Eng. Manuf. 227 (2013) 1138–1147.
[8] F. Wang, S. Williams, P. Colegrove, A.A. Antonysamy, Microstructure and mechanical properties of wire and arc additive manufactured Ti-6Al-4V, Metall. Mater. Trans. A Phys. Metall. Mater. Sci. 44 (2013) 968–977.
[9] L. Neto, S. Williams, J. Ding, J. Hönnige, F. Martina, Mechanical properties enhancement of additive manufactured Ti-6Al-4V by machine hammer peening, In: Lecture Notes in Mechanical Engineering, Springer, 2020, pp. 121–132. https://doi.org/10.1007/978-981-15-0054-1_13.
[10] X. Xu, S. Ganguly, J. Ding, S. Guo, S. Williams, F. Martina, Microstructural evolution and mechanical properties of maraging steel produced by wire + arc additive manufacture process, Mater. Charact. 143 (2018) 152–162.
[11] X. Zhang, F. Martina, J. Ding, X. Wang, S.W. Williams, Fracture toughness and fatigue crack growth rate properties in wire + arc additive manufactured Ti-6Al-4V, Fatigue Fract. Eng. Mater. Struct. 40 (2017) 790–803.
[12] ER70S-6 – Weld WireWeld Wire. http://www.weldwire.net/weld_products/ww70s-6/.
[13] Mild Steel Welding Alloy ER70S-6 (GMAW) (MIG) ER70S-6 (GMAW) (MIG) Mild Steel Alloy • AWS ER70S-6. www.mathesongas.com.
[14] Lincoln Electric Company, T. LINCOLN ® ER70S-6 WELDING POSITIONS TYPICAL APPLICATIONS. www.lincolnelectric.com.
[15] ER100S-G Data Sheet – Bohler Welding; 2014. www.voestalpine.com/welding.
[16] ER100S-1 Data Sheet – Pinnacle Alloys. www.pinnaclealloys.com.
[17] P. Dirisu, S. Ganguly, A. Mehmanparast, F. Martina, S. Williams, Analysis of fracture toughness properties of wire + arc additive manufactured high strength low alloy structural steel components, Mater. Sci. Eng. A 765 (2019) 138285.
[18] A. Ermakova, A. Mehmanparast, S. Ganguly, A review of present status and challenges of using additive manufacturing technology for offshore wind applications, Procedia Struct. Integr. 17 (2019) 29–36.
[19] American Society for Testing and Materials, ASTME-1820-11: standard test method for measurement of fracture toughness, Annu. B. ASTM Stand. 1–55 (2011), https://doi.org/10.1520/E1820-18.
[20] ASTM Standard E8/E8M-13a, Standard test methods for tension testing of metallic materials, ASTM Int. i (2013) 1–27.
[21] A. Acciaioli, G. Lionello, M. Baleani, Experimentally achievable accuracy using a digital image correlation technique in measuring small-magnitude (< 0.1%) homogeneous strain fields, Materials (Basel) 11 (2018).
[22] International Standard ISO, Metallic materials – Vickers hardness test – Part 1: Test method (ISO 6507–1: 2018), Int. Stand. 1–49 (2018) Doi: ISO 6507-1 : 2018.
[23] T.L. Anderson, Fracture Mechanics: Fundamentals and Application, Taylor & Francis Group, 2005.
[24] A. Shirizly, O. Dolev, From wire to seamless flow-formed tube: leveraging the combination of wire arc additive manufacturing and metal forming, JOM 71 (2019) 709–717.
[25] T. Ron, G.K. Levy, O. Dolev, A. Leon, A. Shirizly, E. Aghion, Environmental behavior of low carbon steel produced by a wire arc additive manufacturing process, Metals (Basel) 9 (8) (2019) 888.
[26] A. Mehmanparast, J. Taylor, F. Brennan, I. Tavares, Experimental investigation of mechanical and fracture properties of offshore wind monopile weldments: SLIC interlaboratory test results, Fatigue Fract. Eng. Mater. Struct. 41 (2018) 2485–2501.
[27] A. Mehmanparast, F. Brennan, I. Tavares, Fatigue crack growth rates for offshore wind monopile weldments in air and seawater: SLIC inter-laboratory test results, Mater. Des. 114 (2017) 494–504.
[28] A. Mehmanparast, C.M. Davies, The influence of inelastic pre-straining on fracture toughness behaviour of Type 316H stainless steel, Eng. Fract. Mech. 188 (2018) 112–125.
[29] A. Mehmanparast, C.M. Davies, D.W. Dean, K.M. Nikbin, Plastic pre-compression and creep damage effects on the fracture toughness behaviour of Type 316H stainless steel, Eng. Fract. Mech. 131 (2014) 26–37.
[30] M.O. Lai, W.G. Ferguson, Fracture toughness of aluminium alloy 7075–T6 in the as-cast condition, Mater. Sci. Eng. 74 (1985) 133–138.
[31] R. Tangestani, G.H. Farrahi, M. Shishegar, B.P. Aghchehkandi, S. Ganguly, A. Mehmanparast, Effects of vertical and pinch rolling on residual stress distributions in wire and arc additively manufactured components, J. Mater. Eng. Perform. 29 (2020) 2073–2084.